The Growth of One-Dimensional $CuPcF_{16}$ Nanostructures on Gold Nanoparticles as Studied by Transmission Electron Microscopy Tomography

Neng Yun Jin-Phillipp,* Tobias N. Krauss, and Peter A. van Aken

Max Planck Institute for Intelligent Systems, Heisenbergstrasse 3, 70569 Stuttgart, Germany

ABSTRACT

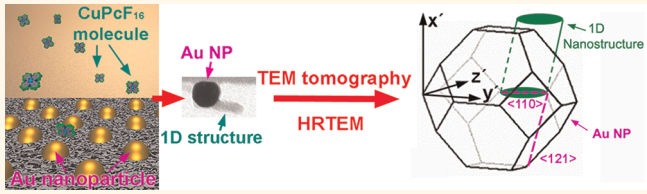

The growth of one-dimensional (1D) fluorinated copper–phthalocyanine ($CuPcF_{16}$) on gold (Au) nanoparticles (NPs) is studied by electron tomography. The shape of the 1D structure and its geometrical relationship with the associated Au NP are determined by a three-dimensional reconstruction analysis combined with high-resolution electron microscopy. The $CuPcF_{16}$ molecules nucleate at the ⟨110⟩ edge of the Au nanoparticle and grow parallel to a {111} facet of the particle along a direction close to ⟨121⟩. This implies that the maximum diameter of the 1D structure is limited by the width of the ⟨110⟩ edge of the Au particle.

KEYWORDS: one-dimensional nanostructure · phthalocyanine · gold nanoparticle · electron tomography · self-organization

Organic electronics progressed with a rapid pace in recent years not only because of the wide range of physical and chemical properties that organic materials offer but also because of the low cost of their possible implementation in devices.[1] Markedly increased research efforts have been devoted in the realization of new organic electronics and optoelectronic devices, such as organic light-emitting devices, organic field effect transistors and organic photovoltaic cells.[2−6] However, the focus has been usually put on thin film structures.[1,7,8] One-dimensional (1D) organic nanostructures, by contrast, open new aspects for multifunctional materials. For example, nanocrystalline donor/acceptor bulk heterojunction devices based on 1D single crystalline organic structures have demonstrated striking increase in efficiency for organic solar cells due to an enormous increase of the donor/acceptor interface.[9,10] One of the fundamental challenges is to guarantee a controlled growth of 1D organic nanostructures with a uniform diameter and separation.[11,12] Recently, it has been reported that organic 1D nanostructures of copper–phthalocyanine ($CuPcF_{16}$) deposited from the vapor phase tend to grow vertically by using templates of gold (Au) nanoparticles (NPs) as illustrated in Figure 1.[13] Further study has shown that the template-induced 1D nanostructure formation is a more general process that appears to other derivatives of the family of phthalocyanines.[14] Since the Au particles can be arranged in a periodic pattern of a certain separation (see Figure 1),[15] the density of the 1D nanostructures is predetermined accordingly. The length of the 1D nanostructures can be tuned by the amount of deposited material and the substrate temperature, and their average diameter seems to be influenced by the size of Au NPs.[14,16] It seems that the 1D nanostructure formation is a strong thermodynamic self-organization process,[14] and its growth is a thermal activated process[13,16] in which Au NPs must play a key role in the nucleation and growth of the 1D nanostructures. To understand the growth of the 1D nanostructures of $CuPcF_{16}$, it is essential to know the shape of the 1D nanostructure and its geometrical relationship with the Au particle. The three-dimensional (3D) faceting morphology of polyhedral NPs can be reconstructed using transmission electron microscopy (TEM)-based tomography on

* Address correspondence to nyjin@is.mpg.de.

Received for review January 24, 2012 and accepted April 6, 2012.

Published online April 06, 2012
10.1021/nn3003482

the nanometer scale.[17,18] The present study, which combines TEM tomography with high-resolution TEM (HRTEM), reveals not only the shape of the 1D nanostructure and the morphology of the Au NP, but also, for the first time, the geometrical relationship between the 1D $CuPcF_{16}$ nanostructure and its associated Au particle. The experimental results from the combination of both techniques provide a detailed 3D insight into the structural properties of the 1D self-organization of $CuPcF_{16}$-molecules on Au NPs, which leads to the proposed growth model of the 1D nanostructures.

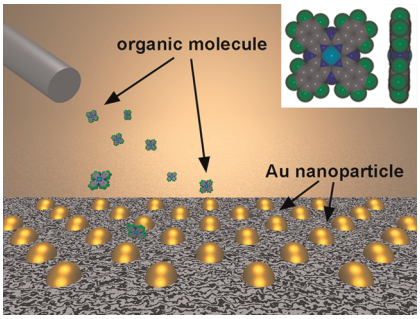

Figure 1. Schematic showing the deposition process of the organic molecules on silicon wafers decorated with arrays of Au NPs. The inset shows the $CuPcF_{16}$ molecule with its front and side-view used in this study.

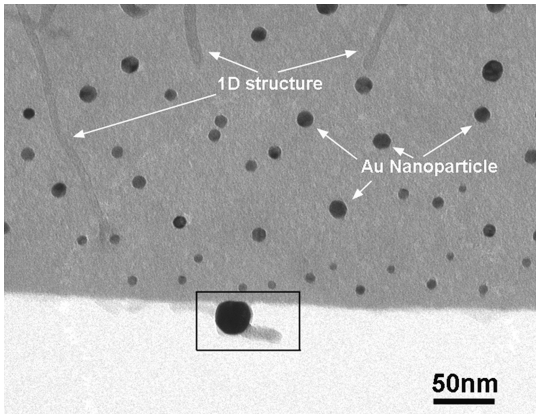

Figure 2. A bright-field (BF) image of 1D $CuPcF_{16}$ nanostructures grown on Au NPs.

TEM TOMOGRAPHY

Figure 2 shows a TEM bright-field (BF) image of the sample (see reference 12 for the growth details), which is in principle a two-dimensional (2D) projection of a 3D volume containing both Au NPs and 1D nanostructures of $CuPcF_{16}$ molecules. The free-standing 1D structure of $CuPcF_{16}$ molecules grown on a Au NP located at the edge of the substrate is our system for this tomographic investigation (within the black rectangle). To reconstruct an object in 3D, which consists in this case of a 1D $CuPcF_{16}$ nanostructure grown on a Au NP, a series of images (projections) must be acquired by tilting the specimen about the eucentric axis of the specimen holder rod as demonstrated in Figure 3a. These images may then be back projected to reconstruct the 3D object as shown in Figure 3b. The details of mathematics can be found in the literature, such as in Frank's book.[19]

For the single-axis tilt geometry, the resolution parallel to the tilt *x*-axis is equal to the original resolution (of the projections). The resolution in the other perpendicular directions is controlled by the number of projections acquired, *N*, and the diameter, *D*, of the volume to be reconstructed by the formulas:[20]

$$d = d_y = d_z = \pi D/N \quad (1)$$

when the projections cover ±90°. In reality, however, because of experimental conditions the tilt range is often limited, which leads to a "missing wedge" of the information. The resolution in the direction parallel to the optic axis, d_z, is further degraded by an elongation factor ε,[21] thus

$$d_z = d_y \times \varepsilon \quad (2)$$

where

$$\varepsilon = \sqrt{\frac{\alpha_{max} + \cos\alpha_{max}\sin\alpha_{max}}{\alpha_{max} - \cos\alpha_{max}\sin\alpha_{max}}} \quad (3)$$

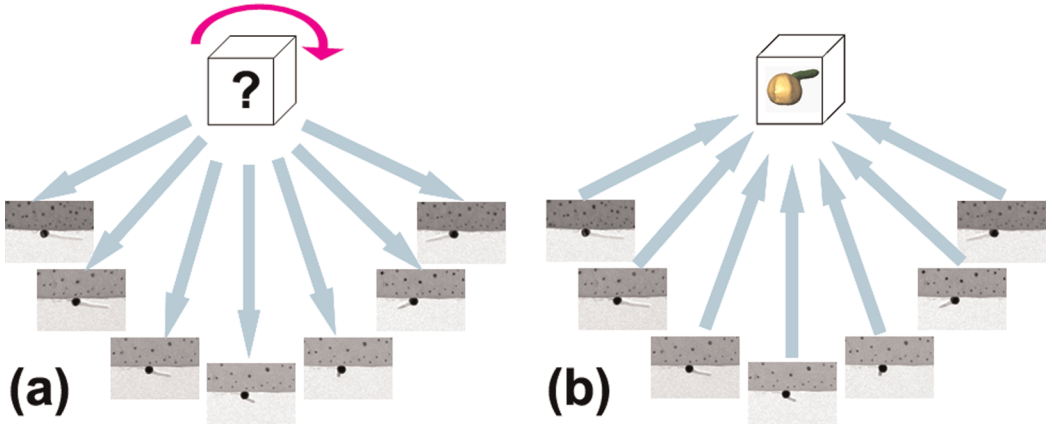

Figure 3. Schematic of electron tomography. (a) Acquisition of a single axis tilt-series of BF images of the system of 1D $CuPcF_{16}$ nanostructure/Au NP taken at various tilting angles. (b) 3D reconstruction of the corresponding system from the tilt-series in schematic (a).

To do such a 3D reconstruction, all images have to be true projections of the structure, that is, the recorded signal must be proportional to the mass−thickness, which the electrons pass through, or at least a monotonically varying function of the mass thickness.[22]

In the present study, the bright-field (BF) imaging mode is employed which is suitable for materials with weak electron scattering such as the $CuPcF_{16}$ structure in this case. For crystalline materials such as crystalline Au, however, the BF contrast of an image depends strongly on the diffraction conditions. Therefore, a strong two-beam condition is avoided in the experiment in order to fulfill the projection principle needed for the reconstruction. Tilt series of BF images were acquired with a Zeiss EM912 microscope operated at 120 kV using the Gatan tomography plug-in for Digital Micrograph at angles ranging from +58° to −58° in 2° steps. The alignment of the tilt series by cross-correlation and the reconstructions using the simultaneous iterative reconstruction technique (SIRT) were performed with the software package Inspect3D of FEI.

HRTEM is carried out at a JEOL 4000FX microscope operated at 400 kV on the same sample after TEM tomography.

RESULTS AND DISCUSSION

Figure 4 parts a, b, and c present three orthogonal views of the reconstruction of a BF tilt series of a free-standing 1D nanostructure of $CuPcF_{16}$ molecules grown on a Au NP, where $x-y$ is the image plane at 0° tilt. Different thresholds of gray levels are chosen for rendering the isosurfaces for $CuPcF_{16}$ and Au respectively. For each viewing direction, the green color indicates the isosurface of the $CuPcF_{16}$ molecule, while the yellow-brown color stands for the isosurface of Au. The missing-wedge effect (see descriptions in the previous section) is apparent, which appears as an

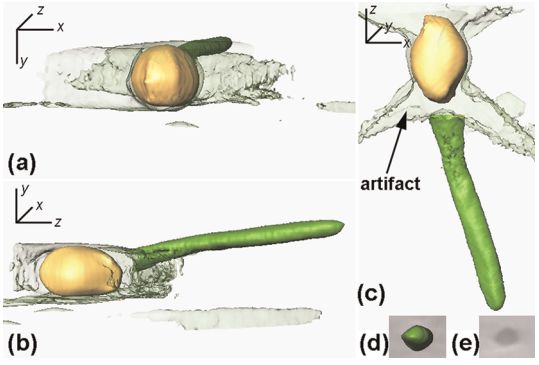

Figure 4. 3D reconstruction of the region marked by the rectangle in Figure 2. Isosurfaces using different thresholds are shown with different color setups, yellow for Au and green for the $CuPcF_{16}$ molecules. The transparent light green region is an artifact due to the "missing wedge" effect and the strong contrast of Au. (a−c) The three orthogonal views of the reconstruction, where $x-y$ is the image plane at 0° tilt; (d) an oblique-slice parallel to the cross-section of the 1D $CuPcF_{16}$ nanostructure; (e) a thin slice parallel to $x-y$ plane from the middle of the reconstructed 1D structure.

elongation of the width of the Au particle along the direction of the electron beam (parallel to the optical axis) represented by the z axis in the images. For the angular range covered by the tilt series, the expected elongation factor ε is 1.61. The streak-shaped feature of half-transparent light green color in the figures, marked with an arrow in Figure 4c, is an artifact which appears when the threshold for rendering the isosurface of the 1D $CuPcF_{16}$ nanostructure is chosen. This artifact is the result of the missing wedge fringes from the strong scattering object of the Au particle. Since the image contrast of Au is some tens of times larger than that of $CuPcF_{16}$, the artifact is especially severe for this system. To avoid this artifact, the cropped region of the isosurface of $CuPcF_{16}$ (green) is used for the later discussions. Figure 4d shows the cross-section of the 1D $CuPcF_{16}$ nanostructure by using an oblique slice perpendicular to the 1D structure.

From the three orthogonal views of the reconstruction it is clear that the 1D nanostructure of $CuPcF_{16}$ molecules is inclined to the z axis. The 3D measurement shows that the angle between the long axis of the 1D structure and z axis is $18 \pm 2°$. Therefore, the elongation factor along z causes only ~5% increase on the diameter of the cross-section. The ratio of the diameters measured from the cross-section is 1.18, which reduces to 1.12 when the elongation along z is taken into account. A thin slice parallel to the $x-y$ plane (Figure 4e) from the middle of the reconstructed 1D structure illustrates a more or less uniform intensity profile across its interior, and volume rendering of the reconstruction shows that the center of the 1D structure is filled. These results reveal that the shape of the 1D $CuPcF_{16}$ nanostructure is a rod (or a wire) with a slight deviation from an ideal cross-sectional disk shape rather than a ribbon or band structure as reported in some studies.[11,12]

To analyze the morphology of the Au NP, oblique slices are employed in the visualization of the 3D reconstruction. Low index planes (facets) of the Au particle are found to be inclined with the original image plane and coordinate axes. Figure 5 shows the three orthogonal views of the same reconstruction of isosurfaces of the system as shown in Figure 4 but along the oblique axes tilted from the original coordinate axes to the low index directions of the Au particle. By intersecting the oblique slice across the Au particle, facets of the Au NP are shown. In Figure 5a,b,c, all three oblique planes are presented with the one parallel to the viewing plane appearing as a gray background and the other two planes, perpendicular to the viewing plane, appearing as light red crosses. For comparison, the original coordinate axes shown in Figure 4 are presented in Figure 5b as the edges of a bounding box. It may be seen that the oblique axes are only slightly tilted from the original coordinate axes. The facets of the Au particle are indicated with white lines. Figure 6 shows a HRTEM image of the same Au NP which

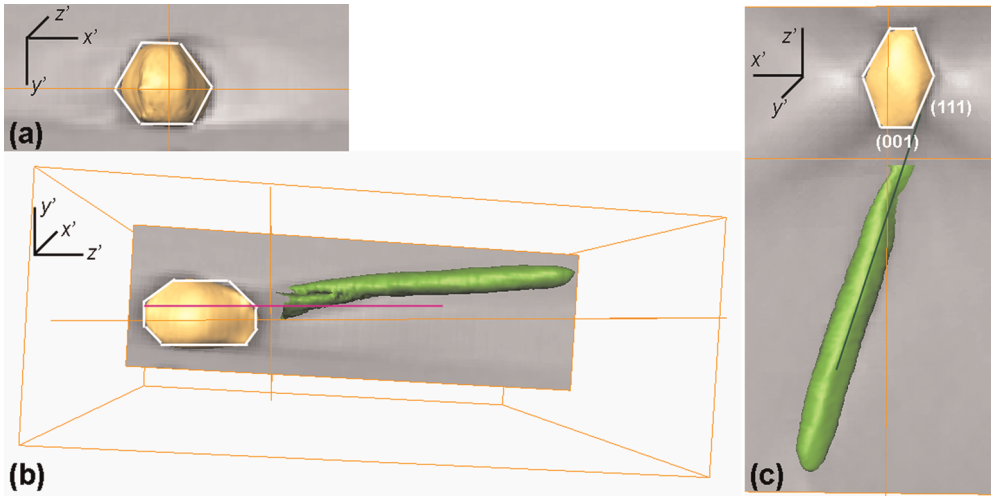

Figure 5. Three orthogonal views of the same reconstruction of isosurfaces of the same 1D $CuPcF_{16}$ nanostructure/Au NP as shown in Figure 4. The viewing directions are along oblique axes tilted from the original coordinate axes (Figure 4) to the low index directions of the Au NP to show the facets of the Au NP (the original coordinate axes shown in Figure 4 are presented in panel b as the edges of the bounding box). All three oblique planes of the reconstruction are presented in each figure with one parallel to the viewing plane appearing as gray background and the two other planes (perpendicular to the viewing plane) appearing as red crosses. The facets of the Au NP are indicated by white lines. The purple line in panel b is along one of the projections of the ⟨121⟩ directions of the Au lattice, whereas the dark green line in panel c is the growth direction of the 1D $CuPcF_{16}$ nanostructure.

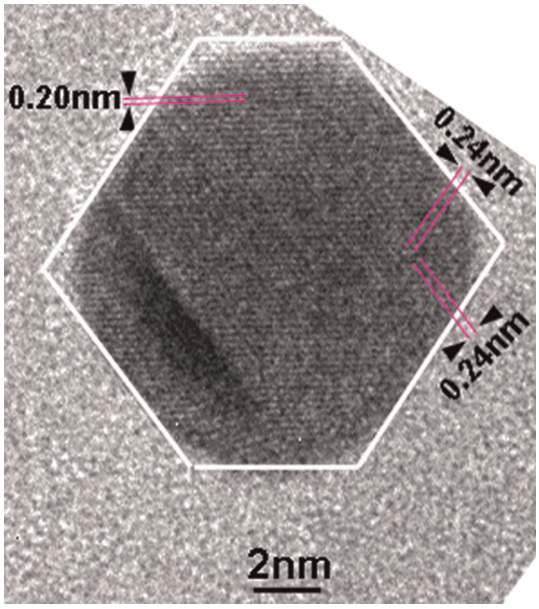

Figure 6. HRTEM image of the Au nanoparticle depicted in Figures 3–5. Its facets are indicated by white lines. The spacings of the three sets of lattice fringes are measured as 0.2, 0.24, and 0.24 nm, respectively, and the latter two sets of fringes make an angle of ~70°.

exhibits a monocrystalline structure with a twin close to its lower-left corner. Its facets are clearly recognizable and are highlighted with white lines. Notice that the particle is somehow roundish at its corners. Three sets of lattice fringes parallel to the facets are seen, as marked with purple lines. Their corresponding spacings are measured as 0.20, 0.24, and 0.24 nm, respectively, which coincide well with the Au lattice spacings 0.2039 nm of {200} and 0.2355 nm of {111} planes. The angle between the two sets of fringes of 0.24 nm spacing is ~70° and the angle between the fringes of 0.20 nm spacing and those of 0.24 nm spacing is 54°, which are close to the expected angles of 70.53° between two Au {111} lattice planes and of 54.73° between {001} and {111} planes, respectively. These results indicate that the facets are {200} and {111}, respectively, and hence the particle is close to the ⟨110⟩ zone axis.

The equilibrium morphology of a particle is determined by the Wulff construction[23] when the particle is sufficiently large (~10 nm). For much smaller particles large deviations from the bulk Wulff model may occur, which leads, for example, to a drop of the (100) surface fraction.[24] The Au NPs under investigation are ~20 nm in size, thus the Wulff construction applies. For an fcc metal such as Au, the construction leads to a morphology of a truncated octahedral enclosed by close packed {111} planes and {100} planes of lowest surface energies, as sketched in Figure 7a. The projections of the truncated octahedral onto the {110} and {100} image planes are shown in Figure 7b and 7c, respectively. The Au NP shown in Figure 6 is a {110} projection and is indeed characterized by the morphology shown in Figure 7b, which confirms that the particle is a truncated octahedron in 3D. The orientation of the particle may be obtained by comparing the shapes of the Au NP in different projections with Figure 7b,c.

From a comparison of the three orthogonal projections along the oblique axes shown in Figure 5 with the schematics of Figure 7 panels b and c and taking the elongation factor of ~1.6 along z (which is close to z') into account, it is clear that the Au particle is viewed along ⟨110⟩ for both Figure 5a and 5c, whereas it is viewed along ⟨100⟩ in 5b. The green line along the

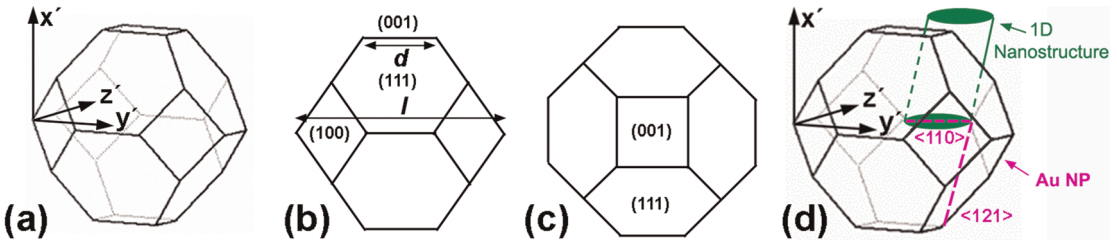

Figure 7. (a) A truncated octahedral, (b, c) the ⟨110⟩ and ⟨100⟩ view of the octahedral in panel a. (d) The geometrical relationship of the 1D $CuPcF_{16}$ nanostructure with its associated Au NP.

growth direction of the $CuPcF_{16}$ 1D structure in Figure 5c is therefore parallel to the (111) facet of the Au particle. Note in Figure 5 panels b and c that the axis of the 1D structure ends at the edge of the intersection of the (001) and (111) planes, implying a possible nucleation and growth of $CuPcF_{16}$ molecules at the edge of the Au particle. The purple line drawn in Figure 5b is the projection of the ⟨121⟩ direction in the (111) plane of the Au particle. It seems that the growth direction of the 1D structure is only slightly deviated from this direction. Because of the artifact from the 3D reconstruction, details in the interface region of the system can unfortunately not be analyzed.

On the basis of the results of TEM tomography and HRTEM, the following growth model of the 1D $CuPcF_{16}$ nanostructure on Au NPs is proposed, as illustrated in Figure 7d: the $CuPcF_{16}$ molecules nucleate at the ⟨110⟩ edges, the intersections of two {111} facets, of the Au NPs and grow parallel to the {111} facets of the particles along a direction close to ⟨121⟩. The maximum diameter of the 1D structure is thus naturally limited by the width of the ⟨110⟩ edge *d* (see Figure 7b).

The active sites of gold catalysts have been discussed in the field of catalyst research. The adsorption of C═O groups of acrolein and subsequent reaction to allyl alcohol are found preferentially occurring on single crystalline Au particles rather than multiple twinned ones, and the active sites of the gold catalysts have been identified as edges of Au NPs.[25] Our TEM tomography observation confirms that the 1D $CuPcF_{16}$ nanostructure nucleates at the ⟨110⟩ edges of the Au NPs.

According to the Wulff's construction, the equilibrium shape of a free-standing particle is determined by the different surface free specific energies of the crystal, following

$$\frac{\gamma_i}{h_i} = \text{constant} \qquad (4)$$

where γ_i is the surface free specific energy of a surface *i*, and h_i is the distance from the center of the particle to *i* surface.[18] For an fcc structure, at 0 K ($\gamma_{(100)}/\gamma_{(111)}$) ≈ 1.15;[26,27] therefore, the relation between the edge length *d* and the size of the truncated octahedral *l* (Figure 7b) can be solely determined from the geometry as

$$d \approx 0.34l \qquad (5)$$

Hence the diameter of the 1D $CuPcF_{16}$ nanostructure is limited by the size of the Au nanoparticle where the nucleation takes place according to our hypothesis of the growth of the 1D nanostructure of $CuPcF_{16}$ molecules. This provides an explanation to the earlier results on the relation between the diameter of the 1D structure and the size of Au particles.[14]

It should be pointed out that the present tomographic analysis has been carried out on one 1D $CuPcF_{16}$ nanostructure grown on its associated Au NP. To generalize the growth model proposed in this study a statistical analysis on the growth of $CuPcF_{16}$ molecules on Au NPs is needed. However, by checking further TEM images, for example, Figure 5 of reference 14, it can be seen that the geometrical relationship between most Au NPs, which show clear facets, with the 1D $CuPcF_{16}$ nanostructures grown on them are in accordance with the growth model suggested above. It is also interesting to note that the correlation between particle diameter and the width of the 1D structure in the range where a uniform 1D growth takes place (Au NP diameter between 14 and 40 nm as shown in Figure 5d of reference 14) exhibits an excellent agreement with expression (5) given in the present publication.

CONCLUSIONS

The shape of the 1D $CuPcF_{16}$ nanostructure and its geometrical relationship with the associated Au nanoparticle on which it grew are determined for the first time by a 3D reconstruction analysis combined with HRTEM. The results suggest that $CuPcF_{16}$ molecules nucleate at ⟨110⟩ edges of Au nanoparticles and grow parallel to a {111} facet of the particle along a direction close to ⟨121⟩. These imply that the maximum diameter of the 1D structure is limited by the width of the ⟨110⟩ edge of the Au particle.

MATERIALS AND METHODS

Organic 1D nanostructures of $CuPcF_{16}$ molecules deposited from the vapor phase were grown on templates of Au nanoparticles. Tilt series of BF images were acquired with a Zeiss EM912 microscope operated at 120 kV using the Gatan tomography plug-in for Digital Micrograph at angles ranging from +58° to −58° in 2° steps. The alignment of the tilt series by cross-correlation and the tomographic reconstructions using

the simultaneous iterative reconstruction technique (SIRT) were performed with the software package Inspect3D of FEI. HRTEM is carried out at a JEOL 4000FX microscope operated at 400 kV on the same sample after TEM tomography.

Conflict of Interest: The authors declare no competing financial interest.

Acknowledgment. The authors acknowledge financial support from the European Union under the Framework 6 program under the contract for an Integrated Infrastructure Initiative Reference 026019 ESTEEM. N.Y.J. is grateful to Kersten Hahn for his assistance at the Zeiss EM912 Omega microscope.

REFERENCES AND NOTES

1. Forrest, S. R. The Path to Ubiquitous and Low-Cost Organic Electronic Appliances on Plastic. *Nature* **2004**, *428*, 911–918.
2. Klauk, H., Ed. *Organic Electronics*; Wiley-VCH: Weinheim, Germany, 2006.
3. Shirota, Y.; Kageyama, H. Charge Carrier Transporting Molecular Materials and Their Applications in Devices. *Chem. Rev.* **2007**, *107*, 953–1010.
4. Vaeth, K. M. OLED-Display Technology. *Inform. Disp.* **2003**, *19*, 12–17.
5. Peumans, P.; Forrest, S. R. Very High Efficiency Double Heterostructure Copper Phthalocyanine/C60 Photovoltaic Cells. *Appl. Phys. Lett.* **2001**, *79*, 126–128.
6. Shaheen, S. E.; Brabec, C. J.; Sariciftci, N. S.; Padinger, F.; Fromherz, T.; Hummelen, J. C. 2.5% Efficient Organic Plastic Solar Cells. *Appl. Phys. Lett.* **2001**, *78*, 841.
7. de Oteyza, D. G.; Barrena, E.; Ossó, O.; Sellner, S.; Dosch, H. Thickness-Dependent Structural Transitions in Fluorinated Copper–Phthalocyanine (F_{16}CuPc) Films. *J. Am. Chem. Soc.* **2006**, *128*, 15052–15053.
8. de Oteyza, D. G.; Barrena, E.; Zhang, Y.; Krauss, T. N.; Turak, A.; Vorobiev, A.; Dosch, H. Experimental Relation between Stranski–Krastanov Growth of DIP/F_{16}CoPc Heterostructures and the Reconstruction of the Organic Interface. *J. Phys. Chem. C* **2009**, *113*, 4235–4239.
9. Yang, F.; Shtein, M.; Forrest, S. R. Controlled Growth of a Molecular Bulk Heterojunction Photovoltaic Cell. *Nat. Mater.* **2005**, *4*, 37–41.
10. Yang, F.; Forrest, S. R. Photocurrent Generation in Nanostructured Organic Solar Cells. *ACS Nano* **2008**, *2*, 1022–1032.
11. Tong, W. Y.; Djurisic, A. B.; Xie, M. H.; Ng, A. C. M.; Cheung, K. Y.; Chan, W. K.; Leung, Y. H.; Lin, H. W.; Gwo, S. Metal Phthalocyanine Nanoribbons and Nanowires. *J. Phys. Chem. B* **2006**, *110*, 17406–17413.
12. Karan, S.; Mallik, B. Templating Effects and Optical Characterization of Copper (II) Phthalocyanine Nanocrystallites Thin Film: Nanoparticles, Nanoflowers, Nanocabbages, and Nanoribbons. *J Phys. Chem. C* **2007**, *111*, 7352–7365.
13. Mbenkum, B.; Barrena, E.; Zhang, X. N.; Kelsch, M.; Dosch, H. Selective Growth of Organic 1-D Structures on Au Nanoparticle Arrays. *Nano Lett.* **2006**, *6*, 2852–2855.
14. Krauss, T. N.; Barrena, E.; Lohmüller, T.; Kelsch, M.; Breitling, A.; van Aken, P. A.; Spatz, J. P.; Dosch, H. One-Dimensional Phthalocyanine Nanostructures Directed by Gold Templates. *Chem. Mater.* **2009**, *21*, 5010–5015.
15. Glass, R.; Arnold, M.; Blümmel, J.; Küller, A.; Möller, M.; Spatz, P. Micro-Nanostructured Interfaces Fabricated by the Use of Inorganic Block Copolymer Micellar Monolayers as Negative Resist for Electron-Beam Lithography. *Adv. Funct. Mater.* **2003**, *13*, 569–575.
16. Krauss, T. N.; Barrena, E.; Lohmüller, T.; Spatza, J. P.; Dosch, H. Growth Mechanisms of Phthalocyanine Nanowires Induced by Au Nanoparticle Templates. *Phys. Chem. Chem. Phys.* **2011**, *13*, 5940–5944.
17. Xu, X; Saghi, Z; Gay, R; Möbus, G. Reconstruction of 3D Morphology of Polyhedral Nanoparticles. *Nanotechnology* **2007**, *18*, 225501.
18. González, J. C.; Hernández, J. C.; López-Haro, M.; del Río, E.; Delgado, J. J.; Hungría, A. B.; Trasobares, S.; Bernal, S.; Midgley, P. A.; Calvino, J. J. 3D Characterization of Gold Nanoparticles Supported on Heavy Metal Oxide Catalysts by HAADF–STEM Electron Tomography. *Angew. Chem., Int. Ed.* **2009**, *48*, 5313–5315.
19. Frank, J., Ed. *Electron Tomography*; Plenum Press: New York, 1992.
20. Hart, R. G. Electron Microscopy of Unstained Biological Material: The Polytropic Montage. *Science* **1968**, *159*, 1464–1467.
21. Radermacher, M.; Hoppe, W. *Proceedings of the Seventh European Congress on Electron Microscopy*, The Hague, The Netherlands, August 24–29, **1980**; pp 132–133.
22. Jin-Phillipp, N. Y.; Koch, C. T.; van Aken, P. A. Toward Quantitative Core-Loss EFTEM Tomography. *Ultramicroscopy* **2011**, *111*, 1255–1261.
23. Wulff, G. On the Question of Speed of Growth and Dissolution of Crystal Surfaces. *Z. Krist. Miner.* **1901**, *34*, 449–530.
24. Marks, L. D. Particle Size Effects on Wulff Constructions. *Surf. Sci.* **1985**, *150*, 358–366.
25. Mohr, C.; Hofmeister, H.; Radnik, J.; Claus, P. Identification of Active Sites in Gold-Catalyzed Hydrogenation of Acrolein. *J. Am. Chem. Soc.* **2003**, *125*, 1905–1911.
26. Henry, C. R. Surface Studies of Supported Model Catalysts. *Surf. Sci. Rep.* **1998**, *31*, 231–325.
27. Shi, A. Effects of Adsorption on Equilibrium Crystal Shape: A Zero-Temperature Calculation. *Phys. Rev. B* **1987**, *36*, 9068–9081.